Is There a Ready-Recipe for Hard Carbon-Electrode Engineering to Enhance Na-Ion Battery Performance?

Joanna Conder, Claire Villevieille, Jean-Marc Le Meins, Camélia Matei Ghimbeu

Is there a ready-recipe for hard carbon-electrodes engineering to enhance Na-ion batteries performance?

*Joanna Conder[1,2], Claire Villevieille[3], Jean-Marc Le Meins[1,2], Camélia Matei Ghimbeu[1,2,4]**

[1]*Université de Haute-Alsace, Institut de Science des Matériaux de Mulhouse (IS2M), CNRS UMR 7361, F-68100 Mulhouse, France*

[2]*Université de Strasbourg, F-67081 Strasbourg, France*

[3] *Univ. Grenoble Alpes, Univ. Savoie Mont Blanc, CNRS, Grenoble INP, LEPMI, 38000 Grenoble, France*

[4] *Réseau sur le stockage électrochimique de l'énergie (RS2E) CNRS FR3459, 33 Rue Saint Leu, 80039 Amiens Cedex, France*

** E-mail: camelia.ghimbeu@uha.fr*

ABSTRACT

Hard carbon (HC) materials are commonly used as anode materials in Na-ion batteries. In most of the cases, their electrochemical performance is correlated only to their physicochemical properties, and the impact of the electrode additives (binders–conductive agent) and electrolyte is often neglected. In this work, a systematic study is performed to understand the role of electrode/electrolyte engineering on HC initial Coulombic efficiency (iCE), specific capacity, and cycle stability. Four HCs obtained by pyrolysis of several biopolymers, i.e., cellulose (HC-Cell), chitosan (HC-Chs), chitin (HC-Cht), and lignin (HC-Lig), are used. The binder was found to have an important impact on the electrochemical performance, with PVDF resulting in better performance than CMC. The carbon black additive had no significant impact on CMC-based electrochemical performance while it boosted the electrochemical performance of PVDF-based electrodes. For an optimized formulation (PVDF/carbon black), the best HC performance in $NaPF_6$ in 1 EC:DEC was delivered by HC-Cell (83% iCE, 332 mAh g^{-1} at C/10, and 97% retention). This was attributed to its large graphene interlayer space, high purity, and low surface area. HC-Cht and HC-Chs exhibited similar good electrochemical performance (~280 mAh g^{-1}) whereas the use of HC-Lig resulted in low iCE and capacity fading overcycling due to the high level of impurities in its structure. This could be overcome by changing the electrolyte salt, by using $NaClO_4$ (76% retention) instead of $NaPF_6$ (52% retention). Based on the obtained results, the electrochemical performance could be correlated with the HC physicochemical properties and binder/conductive additive. It could be demonstrated that careful electrode engineering combined with proper electrolyte selection and tuned HC properties allowed all investigated materials achieving reasonable iCE (up to 83%), high specific capacity (~280 to 332 mAh g^{-1}), and high-capacity retention (72–97% after 50 cycles).

Keywords: *hard carbon; anodes; sodium ion batteries; chitosan; chitin; cellulose; lignin;*

GRAPHICAL ABSTRACT

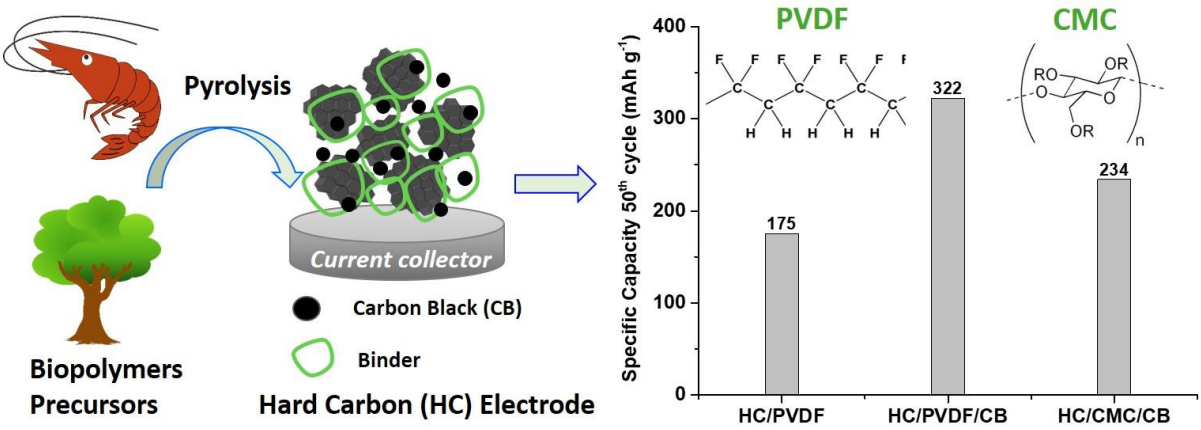

1. INTRODUCTION

Na-ion batteries (NIBs) gained increased popularity in the previous years owing to (i) the availability of sodium resources, (ii) their potentially lower cost compared to current Li-based technologies, and (iii) the recent advances in engineering leading to increase in the overall power-based performance compared to Li-ion batteries. Among the negative electrodes, hard carbons (HCs) became very promising thanks to their appealing electrochemical performance (~300 mAh g^{-1} specific capacity), [1-3] approaching that of graphite (372 mAh g^{-1}) [4] in lithium ion batteries (LIB_s). In terms of electroactive materials, the abundant, renewable, and sustainable precursors used for the materials synthesis constitute key criteria for large scale implementation.

Indeed, many works explored various resources (biomass waste, biopolymers, synthetic polymers, etc.) [5] for HC production via pyrolysis approaches to improve the HC electrochemical performance and long-term cycling stability. Along with the synthesis and postsynthesis conditions (pyrolysis temperature, doping, activation, washing, and so forth), the HC properties (structure, porosity, morphology, surface functionalities, etc.) could be tuned and their impact on the electrochemical behavior investigated. [6-10]. Quite recently, several parameters such as HC graphitic interlayer space, specific surface area (SSA), open/closed porosity, and amount/nature of functional groups/dopants have been pointed out to be crucial to ensure a reasonable initial columbic efficiency (iCE), specific capacity, and long-term capacity. Although a straightforward correlation between the HC features and electrochemical performance vs Na metal is difficult to draw due to the lack of standard protocol between the laboratories, some general trends can be provided. For most of the precursors, the increase in the pyrolysis temperature (up to approximately 1400–1600 °C temperature range) leads to a gradual decrease in the specific surface area, the interlayer layer space, the number of functional

groups, and defects, [5, 11] and this has a positive impact on the iCE and specific capacity. [5, 11-14]. Increasing the pyrolysis temperature (higher than 1600 °C) leads to a decrease in the specific capacity due to the limited interlayer space[15, 16] hindering the Na-ion uptake. In addition, for a given pyrolysis temperature, the precursor itself plays an important role in defining the electrochemical performance of the hard carbon. [5] For this reason, the relationship among the HC electrochemical performance, its precursor, and synthesis conditions was extensively studied and reviewed in detail in several articles. [1, 3, 17, 18]

To date, only a few papers are reporting the impact of the electrode engineering (in particular binder/solvent selection, addition of conductive carbon), electrolyte/additive type, and cycling conditions, although this aspect is still a crucial step when it comes to battery electrochemical performance. These factors may lead to different electrochemical results which are not directly related to the active material itself, although many times these differences have been attributed to HC properties. For instance, many papers reported that HCs derived from cellulose have capacities and iCE values that vary significantly. [19-22] These discrepancies might be due to (i) the lack of standardization, (ii) the electrode engineering, (iii) the electrolyte composition, and (iv) the Na metal used as a counter electrode. For the latter, the long-term cycling stability is quite often discussed and attributed to HC whereas it was demonstrated that the Na metal counter electrode is mostly responsible for the electrochemical performance decay. [23-26]

For the electrode formulation, the most commonly used binder is the polyvinylidene difluoride (PVDF) owing to its high binding strength and stability; [27, 28] however, it requires formulation with organic solvents such as *N*-methyl-2-pyrolidone (NMP) whose toxicity raises concerns. Other green alternatives, based on nonfluorinated polymers and biopolymers formulated in water, have been explored as well. [28, 29] Dahbi et al. [30] investigated the impact of binder on the electrochemical performance of a commercial HC using 1 M $NaPF_6$/PC electrolyte with or without electrolyte additive (fluoroethylene carbonate, FEC). In their work, the

carboxymethylcellulose (CMC) binder delivered better specific capacity and cycle stability than PVDF. This has been ascribed to the formation of a uniform passivation layer of CMC on the carbon surface which stabilizes the electrode and provides better electrochemical performance. For the PVDF binder, the authors observed the formation of NaF species coming from the binder degradation, which contributed to lower HC particle cohesion, their electrical isolation, and the increase of the electrode polarization. When the FEC additive was employed, capacity retention was improved for the electrodes containing PVDF, whereas for CMC-based electrodes, the delivered specific capacity was worse. In another study, Fan et al. [31] compared , sodium polyacrylate (Na-PAA) and PVDF binders, using nitrogen doped carbon nanotubes (N-CNTs) and $NaClO_4$ in EC/PC electrolyte. The electrodes containing Na-PAA delivered higher initial Coulombic efficiency (61.2%) compared to PVDF (45%), higher specific capacity, and better capacity retention (76.0% vs. 28.5%) after 300 cycles. The authors explained the improved electrochemical performance of Na-PAA by the formation of a homogeneous passivation layer on the HC particle surface that lowers internal resistance and improves adhesion of the electrode to the Cu-foil current collector. The influence of molecular weight of Na-PAA has been investigated as well, and the binding capability was found to diminish with the molecular weight. More recently, Darjazi et al. [32] explored several nontoxic water processed binders, i.e., CMC, Na-aliginate (Alg), and poly(acrylic acid, PAA) vs PVDF using coffee ground-derived HC and $NaClO_4$ in EC:PC electrolyte. The SEM investigation of the pristine electrodes showed several features depending on the binder, homogeneous particle distribution for CMC, some aggregates for PAA and Alg, and very poor particle distribution and cracks for the PVDF-based electrode. The slower evaporation rate of NMP solvent in the latter case could be responsible for the observed cracks. The iCE delivered by the Alg and PAA electrodes was higher than for CMC and PVDF. In terms of capacity retention, the Alg performed the best with 98% retention, vs 83.7% for PAA, 77% for CMC, and 76.3% for PVDF after 100 cycles. The

improved performance in the case of Alg was ascribed to lower resistance of the electrode, a more uniform passivation layer, and better contact between the particles and the current collector as compared to PVDF.

The electrolyte is also of great importance to improve the electrochemical performance. Bommier and Ji [27], reviewed about 500 papers to elucidate the role of the electrolyte. $NaClO_4$ is the most used salt in Na-ion batteries compared to $NaPF_6$. It was difficult to draw a clear conclusion from this study due to the lack of standardization between the studies. The same concerns were relevant to the solvent choice; the most commonly used solvents are ethylene carbonate (EC)/dimethylcarbonate (DEC), but no clear conclusion on the capacity retention could be drawn, while PC seems detrimental to the iCE. Finally, the effect of additive has been studied. FEC reported first by Komaba et al. [33] was the most commonly used in several studies. However, the beneficial role of FEC on the iCE and long-term capacity could not be demonstrated, as reviewed elsewhere. [27]

Based on the aforementioned literature, there is still a lack of studies regarding the relationship between the electrode formulation (HC–binders–carbon additives) and the electrolytes. This work proposes a systematic study of the impact of binder, carbon black, and electrolyte type on the HC electrochemical performance. For a given formulation/electrolyte couple, there is always a trend of the electrochemical performance delivered by HC materials. However, this trend is not the same when the formulation/electrolyte is changed. This highlights both the impact of HC properties–electrode formulation and electrolyte on the electrochemical performance. It should be emphasized that an appropriate electrode formulation/electrolyte couple allows good electrochemical performance for all HC materials. This approach led us to maximize the electrochemical performance.

2. EXPERIMENTAL

2.1. Materials synthesis

Hard carbon materials were synthesized by a pyrolysis process using four biopolymer precursors, namely, chitosan, chitin, cellulose, and lignin. All precursors (chitosan of medium molecular weight, chitin from shrimp shells, medium cellulose fibers, and lignin alkali/lignin kraft) have been purchased from Sigma-Aldrich and used without further modification.

In a typical synthesis, 3–4.5 g of precursor was placed in an alumina boat and heat-treated with a heating rate of 5 °C min^{-1} under argon at 1300 °C. Once the temperature was reached, it was held for 1 h to ensure homogeneous carbonization of the entire mass. After the pyrolysis step, the sample was naturally cooled down to room temperature and ground for further characterization. The as-obtained hard carbons from chitosan, chitin, cellulose, and lignin are denominated HC-Chs, HC-Cht, HC-Cell, and HC-Lig, respectively.

2.2. Material characterization

The HC structural features were determined by several complementary techniques. X-ray diffraction (XRD) patterns were recorded with a Bruker D8 Advanced A25 diffractometer. The instrument was equipped with a LynxEye XE-T high-resolution energy-dispersive 1-D detector (Cu $K\alpha_{1,2}$) and worked in Bragg–Brentano θ–θ geometry. The general conditions of acquisition were the following: angular domain of 10° to 90° 2θ, step size 0.010°, total measurement time of 1 h 8 min, and variable divergence slit mode used for a constant illuminated area of 15 mm. The graphitic interlayer space (d_{002}) was determined based on the (002) diffraction peak position using the Bragg law. The crystallite size (L_c) was calculated using the Scherrer equation [34] considering the (002) graphite peak position and full-width at half-maximum (fwhm). Local structural information was obtained by Raman spectroscopy with a LabRAM BX40 (Horiba

Jobin-Yvon) spectrometer equipped with a He–Ne excitation source (532 nm wavelength). For each material, nine spectra were recorded to ensure good representation of the HC structure. The average spectrum was used for the calculations. Normalization based on the G band and fitting with a Lorentzian function in Origin software was carried out to determine the I_D/I_G ratio. For the latter calculations, the area under the peaks was considered and not the intensities of the respective peaks. The local structure was obtained by high-resolution transmission electron microscopy (HRTEM) with a JEOL ARM-200F instrument (200 kV). The HC bulk chemical composition was determined by energy-dispersive X-ray spectroscopy (EDX) analysis by means of a FEI Quanta 400 scanning electron microscope equipped with a JED 2300 EDX detector. Chemical analysis in the extreme surface (∼10 nm) was performed with an X-ray photoelectron spectroscope (VG SCIENTA Model SES-2002). Bulk surface chemistry (type and quantity of functional groups) of carbon materials was assessed by temperature-programmed desorption coupled with mass spectrometry (TPD-MS). A small amount of carbon was vacuum heat-treated with a heating rate of 5 °C min^{-1} up to 950 °C. The oxygen-based functional groups were decomposed with the release of CO and CO_2 gases depending on their thermal stability. Additionally, the active surface area (ASA) was obtained by performing a second TPD-MS on the already vacuum "cleaned" material and prior to being exposed to O_2 for 10 h at 300 °C. More details about the TPD-MS procedure can be found elsewhere. [11, 35]

Textural properties of HC were determined by measuring the N_2 adsorption/desorption isotherms with an ASAP 2420 instrument (Micromeritics) using N_2 as adsorbate at 77 K. Complementary CO_2 adsorption isotherms were measured with an ASAP 2020 instrument (Micromeritics) using CO_2 adsorbate at 273 K. Prior to the analyses, the HCs were outgassed at 300 °C for 12 h on the degassing port to remove the water and other molecules from the pores. In addition, 2 h of outgassing on the analysis port was conducted to remove the backfilled gas molecules. The specific surface area (SSA) was assessed by the Brunauer–Emmett–Teller

(BET) method, in the relative pressure ranges 0.05–0.3 and 0.01–0.03 for N_2 and CO_2, respectively.

2.3 Electrode formulation

HC electrodes were prepared using four hard carbon materials and different formulations. First, the materials were formulated without carbon black using organic and water based-solvent. Typically, the HC was mixed with the binder, i.e., polyvinylidene fluoride (PVDF, HSV-900, Arkema) in *N*-methyl-2-pyrrolidone (NMP, Alfa Aesar), in a weight ratio for hard carbon:binder of 90:10. This refers to the organic-based formulation. A water-based procedure using carboxymethylcellulose (CMC, Alfa Aesar) was employed as comparison. The obtained electrodes (8) are labeled as HC-XXX/PVDF and HC-XXX/CMC (where XXX- is the abbreviation of precursor used to synthesize the HC). Second, the materials were formulated with carbon black (SuperP, Imerys), in a weight ratio, hard carbon:binder:carbon black of 80:10:10, respectively. The resulting electrodes (8) are labeled as HC-XXX/PVDF/SuperP and HC-XXX/CMC/SuperP. The as-obtained slurries were mixed with a turbo stirrer and cast onto aluminum foil by a doctor-blading technique. Next, the electrodes were vacuum-dried at 80 °C for 12 h and calendared to a thickness of ∼100 μm. They were punched to a diameter of 13 mm and dried under dynamic vacuum at 80 °C for 12 h prior to being inserted in an Ar-filled glovebox. The HC-based electrode loading was between 4.5 and 6.0 mg/cm^2

2.4 Electrochemical characterization.

Coin-type cells have been assembled with HC as a negative electrode, and sodium metal as reference and counter electrodes, prepared following ref [23], and with a glass-fiber separator (Whatman GF/D). The latter was soaked with 500 μL of electrolyte and 1 M sodium hexafluorophosphate ($NaPF_6$) in 1:1 v/v% mixture of ethylene carbonate (EC) and diethyl carbonate (DEC) (Kishida Chemical, battery grade). For the sake of comparison, 1 M sodium

perchlorate ($NaClO_4$) in the same solvent mixture, EC/DEC, has been used for some electrodes. The cells were galvanostatically discharged to 5 mV at a current initially corresponding to C/10 rate. Once the low cutoff potential was reached, the discharge continued at a constant voltage for additional hour. The same constant current/constant voltage protocol was applied during subsequent charging from 5 mV up to 1.2 V. After the first two cycles, the current was increased, and the cells continued cycling at a C/5 rate. All cells were cycled at 25 °C. From this point onward, all potentials are quoted with respect to Na^+/Na used as a reference electrode. All the hard carbons, electrode formulations, and electrolytes used for the electrochemical tests are summarized in Table 1

Table 1: Electrode formulations including the hard carbon active material, the conductive additive and the binder, as well as the electrolytes used in this work.

<table>
<tr><th rowspan="2">Hard Carbon</th><th colspan="2">Electrode Formulation</th><th rowspan="2">Electrolyte</th></tr>
<tr><th>Conductive additive</th><th>Binder</th></tr>
<tr><td rowspan="15">HC-Chs
HC-Cht
HC-Cell
HC-Lig</td><td rowspan="8">Without SuperP</td><td>PVDF</td><td rowspan="14">1M $NaPF_6$ in EC:DEC</td></tr>
<tr><td>HC-Chs/PVDF
HC-Cht/PVDF
HC-Cell/PVDF
HC-Lig/PVDF</td></tr>
<tr><td>CMC</td></tr>
<tr><td>HC-Chs/CMC
HC-Cht/CMC
HC-Cell/CMC
HC-Lig/CMC</td></tr>
<tr><td rowspan="7">With SuperP</td><td>PVDF</td></tr>
<tr><td>HC-Chs/PVDF/SuperP
HC-Cht/PVDF/SuperP
HC-Cell/PVDF/SuperP
HC-Lig/PVDF/SuperP</td></tr>
<tr><td>CMC</td></tr>
<tr><td>HC-Chs/CMC/SuperP
HC-Cht/CMC/SuperP
HC-Cell/CMC/SuperP
HC-Lig/CMC/SuperP</td></tr>
<tr><td>HC-Lig/PVDF/SuperP
HC-Chs/PVDF/SuperP</td><td>1M $NaClO_4$ in EC:DEC</td></tr>
</table>

3. RESULTS AND DISCUSSION

3.1 Material Characterization

Four HC materials and electrodes were obtained by pyrolysis of chitosan, chitin, cellulose and lignin biopolymers at 1300 °C, according to Scheme 1.

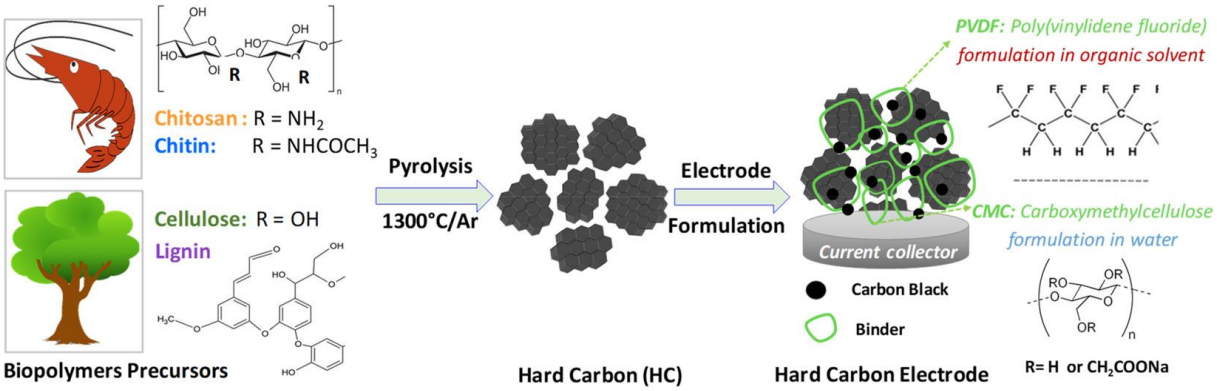

Scheme 1: Synthesis of hard carbon materials by pyrolysis of biopolymers and the electrode preparation.

The thermal decomposition behavior and the conversion yield of biopolymer into carbon were studied by thermogravimetric analysis, TGA (Figure S1, Supporting Information). They are strongly dependent on the precursor chemical composition (Table S1, Supporting Information) and structure (Scheme 1), as explained in detail in the SI. Briefly, the C-yield determined at 900 °C (Table 2) is the highest for lignin precursor (40 wt %), followed by chitosan (27 wt %) and finally by chitin and cellulose (10–12 wt %). The high C-yield is an important advantage to reduce the production cost and the environmental impact (less gas release).

The HC morphology and the particle size distribution depend on the initial precursor morphology. All materials present a random particle shape as illustrated in the SEM images (Figure S2, Supporting Information). However, the size of the particles is rather different from one HC to another; i.e., the HC-Chs has a large particle size between 300 and 600 µm, and HC-Cht presents a lower particle size (100–200 µm) while for HC-Lig and HC-Cell, the particle

sizes are smaller than 150 μm. The morphology of the particles as well as the particle size distribution are two crucial parameters when it comes to the electrochemical performance and the electrode engineering. We reported earlier that smaller particles are more preferable to obtain homogeneous electrodes and improved electrochemical performance. [36]

HC structure was verified by several complementary techniques (XRD, Raman, and HRTEM). The graphitic/disordered domains and the interlayer space (d_{002}) are considered as one of the main sites of Na^+ insertion, and they are strongly related to the carbon precursor. [13, 15, 37, 38] The XRD diffractograms (Figure 1a) show the presence of three diffraction peaks at ~23°, 44°, and 80° 2θ. Their position corresponds to the (002), (101), and (110) diffraction plane of hexagonal graphite. However, for all the HCs, the (002) peak position is far from that of ideal graphite (26°), and the peak is very broad, suggesting disordered-like materials. The d_{002} interlayer space (Table 2) was found to be the highest for HC-Cell (3.81 Å), followed by HC-Lig (3.70 Å), HC-Chs (3.65 Å), and HC-Cht (3.60 Å). The obtained values are higher than that for the graphite (3.35 Å) which should ensure efficient Na-ion insertion. Some theoretical studies estimate that a d_{002} of at least 3.7 Å is ideal for this purpose. [39] The graphite staking height or crystallite size (L_c) varies in the opposite way compared to d_{002}; i.e., the lowest value is found for HC-Cell (9.8 Å) whereas the highest value is determined for HC-Cht (12.4 Å). This corresponds to 3–4 graphitic layers together in HC materials.

In addition to the peaks assigned to graphite phase, some small peaks are observed for HC-Chs and HC-Lig. Although a precise identification of the impurities is always difficult since the peaks are rather small, calcium carbonate ($CaCO_3$, COD 9015481), sodium sulfide (Na_2S, COD 2106220), and sodium pyrosulfate ($Na_2S_2O_7$, COD 1535121) are detected for HC-Chs while sodium sulfate (Na_2SO_4, COD 2107319) and potassium carbonate (K_2CO_3, COD 9009644) seem to be present in the case of HC-Lig.

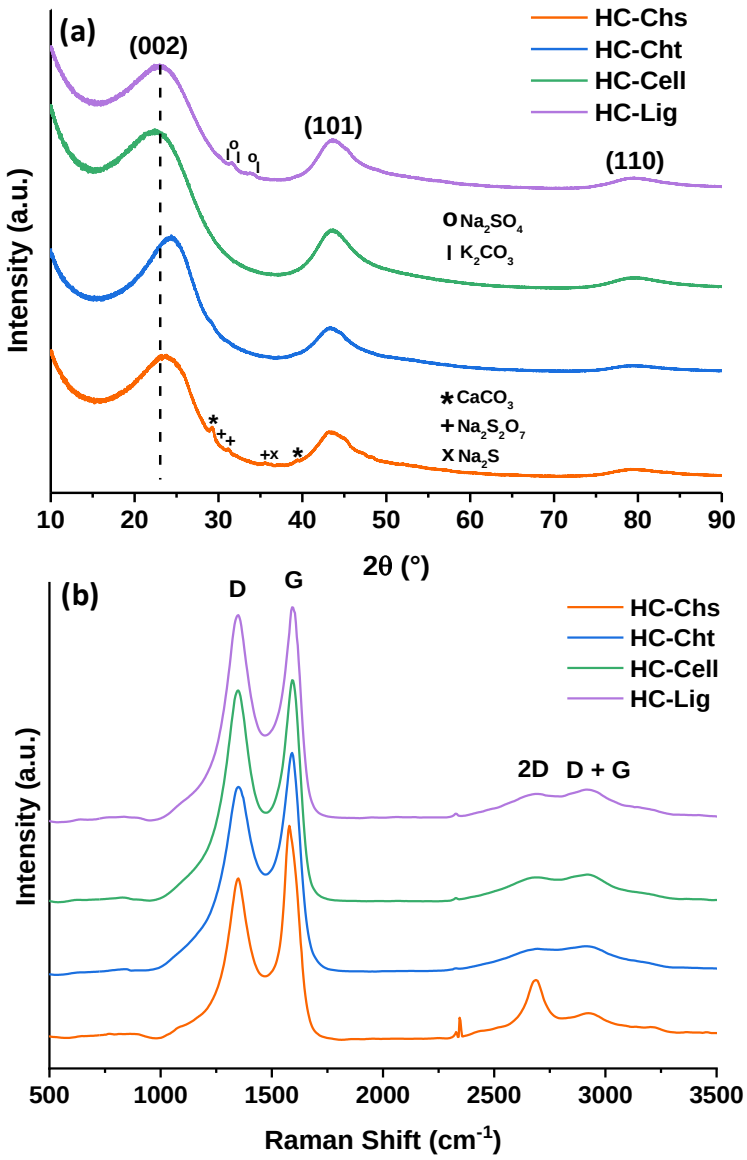

Figure 1: Cu ($K\alpha_{1,2}$) XRD-diffractograms (a); impurities are partially indicated (only strongest reflexions) and averaged Raman spectra (b) of hard carbon materials: HC-Chs, HC-Cht, HC-Cell and HC-Lig.

HC-Cht and HC-Cell also contain some impurities, i.e., (Ca-based) and (Si-based), respectively, as shown by XPS analyses. These are not detected by XRD, probably due to their low amount (~1 at. %) and/or a lack of crystallinity. Some of these impurities may contribute to local graphitization of hard carbon and thus to narrowing of the d_{002} interlayer space. [8, 40] As observed for HC-Chs (TEM image, Figure 2a), d_{002} might as well be affected by the localization of impurities, especially their confinement between graphene planes. Moreover, an important

factor dictating the d_{002} is the precursor itself, i.e., its structure and chemical composition. [5] All these contribute to the different d_{002} values observed for the materials.

The inorganic impurities may lower the electrochemical performance of HCs since they diminish the electronic conductivity of carbon materials and are not cycling; thus, "dead weight" is carried on. [8] They might also contribute to the irreversible reactions with the electrolyte and thus to lower initial Coulombic efficiency and cycle stability, as previously pointed out. [8, 40-42]

Table 2: Physico–Chemical Properties of HC Including the C-Yield Obtained by TGA, the Interlayer Space (d_{002}) and the Crystallite Size (L_c) Determined by XRD, the BET Surface Area Obtained by N_2 and CO_2 Adsorption (S_{BET} N_2 and S_{BET} CO_2), the C and O Amounts Obtained by XPS, the Amount of Oxygen-Based Groups (CO_x), and the Active Surface Area (ASA) Assessed by TPD-MS

Material	C-yield wt.%	d_{002} Å	Lc Å	I_D/I_G	$S_{BET}N_2$ m^2 g^{-1}	$S_{BET}CO_2$ m^2 g^{-1}	C at.%	O at.%	COx mmol g^{-1}	ASA m^2 g^{-1}
HC-Chs	27	3.65*	11.2*	1.43	2.5*	<1	78.93	14.88	0.084	1.8*
HC-Cht	12	3.60*	12.4*	1.98	110*	72	96.22	2.84	0.145	11*
HC-Cell	10	3.81	9.8	2.03	5.1	74	95.61	3.38	0.108	8.2
HC-Lig	40	3.70	10.4	1.79	1.6	< 1	83.91	11.81	0.214	5.0

*- taken from Ref. [41].

More local structural insights were obtained by Raman spectroscopy (Figure 1b). Two intense peaks are seen at ∼1350 and 1590 cm^{-1} and associated with the D (defect) and G (graphite) bands, respectively. The I_D/I_G ratio is usually employed to describe the degree of structural disorder. An example of fitted Raman spectrum is provided in Figure S3a (Supporting Information). The HC-Chs present the lowest I_D/I_G ratio (1.43) indicating higher structural organization. This is also confirmed by the width of D and G bands and by the presence of an additional peak, known as 2D. The latter peak is observed only for this material and associated

with graphitic domains. Its intensity varies depending on the analyzed area (Figure S3b, Supporting Information), suggesting a heterogeneous structure composed of disordered and graphitic-like domains. For the other materials, the I_D/I_G ratio is higher than that for HC-Chs and varies in the following order: HC-Chs < HC-Lig < HC-Cht < HC-Cell (Table 2). This order is in good agreement with the d_{002} evolution, except for HC-Cht which despite the low d_{002} value presents a high I_D/I_G ratio (1.98).

Interestingly, a closer look at the structure of HC-Chs by HRTEM (Figure 2) reveals a presence of disordered carbon with randomly oriented graphene layers and highly graphitic zones, characterized by long graphitic domains with several stacked graphene layers (~10–15 layers).

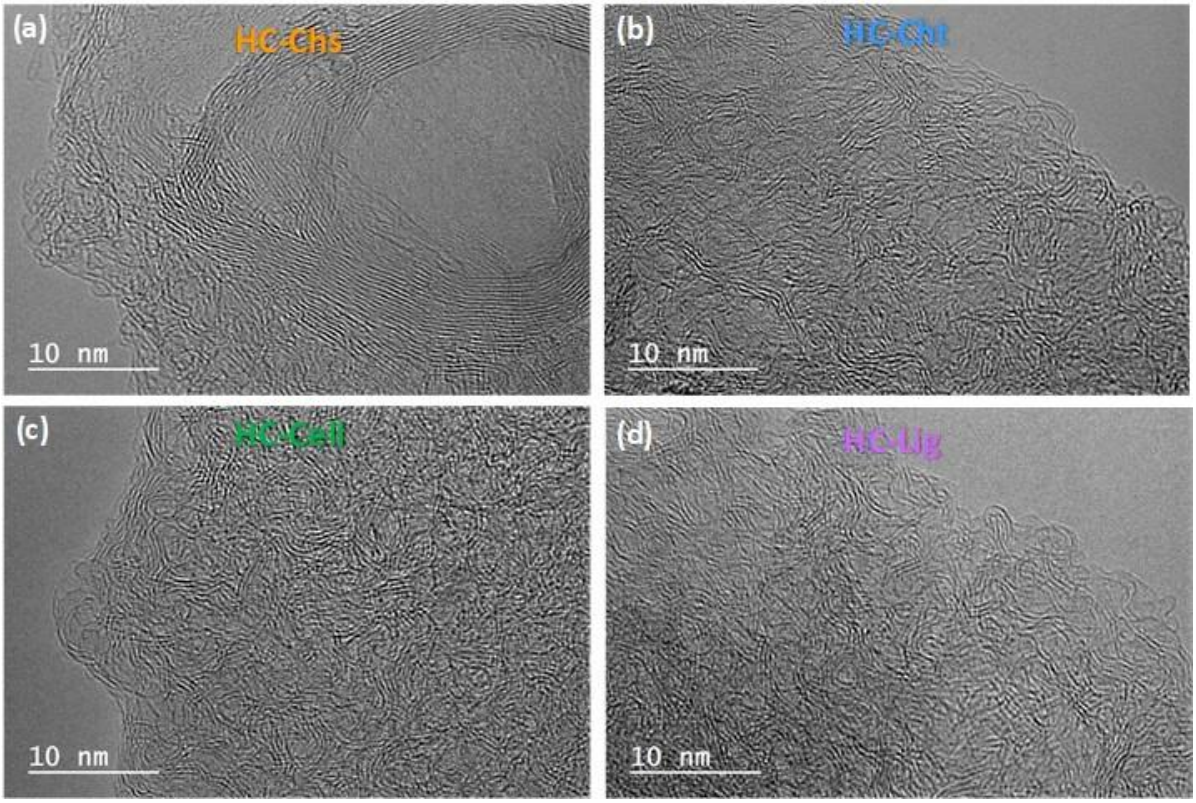

Figure 2: HRTEM images of hard carbon materials: (a) HC-Chs, (b) HC-Cht, (c) HC-Cell and (d) HC-Lig.

The presence of highly graphitic domains in this material is a consequence of catalytic reactions occurring between the carbon structure and the Ca-based inorganic impurities present therein.

[40, 41] Moreover, closed pores can be seen inside the graphitic concentric layers. Nevertheless, based on all analyzed images (not shown here), the disordered zones are more predominant that the graphitic ones. For HC-Cht, HC-Cell, and HC-Lig, a typical HC structure is observed, composed of pseudographitic domains with 2–4 short and curved stacked graphene layers, and disordered-like domains.

The porosity of HC is rather complex due to the presence of closed and open pores. The former ones are seen on HRTEM images of HC-Chs (Figure 2a) but are difficult to observe for the other HCs. These types of pores tend to be more developed at a pyrolysis temperature higher than 1300 °C, used in this study. According to several studies, [43-46] Na-ion insertion into closed pores might occur within the low-voltage potential plateau during cycling. As for the open porosity, it can be accessed by gas adsorption and provide relevant information about the specific surface area, pore size, and pore volume. These textural features are known to contribute to several electrochemical parameters such as (i) the wettability of the material by the electrolyte, (ii) the decomposition of the electrolyte on the external carbon surface, (iii) the formation of a solid electrolyte interphase (SEI), and (iv) the trapping of Na^+ in the pores. [47, 48] Therefore, the proper determination of porosity is of paramount importance. The N_2 adsorption/desorption isotherms (Figure 3a) indicate that HC-Chs, HC-Cell, and HC-Lig adsorb a very small amount of N_2 volume, which can be translated into a very low specific surface area, S_{BET} between 1.6–5.1 $m^2\ g^{-1}$. A low S_{BET} is important to limit the electrolyte degradation and to avoid a thick SEI formation.

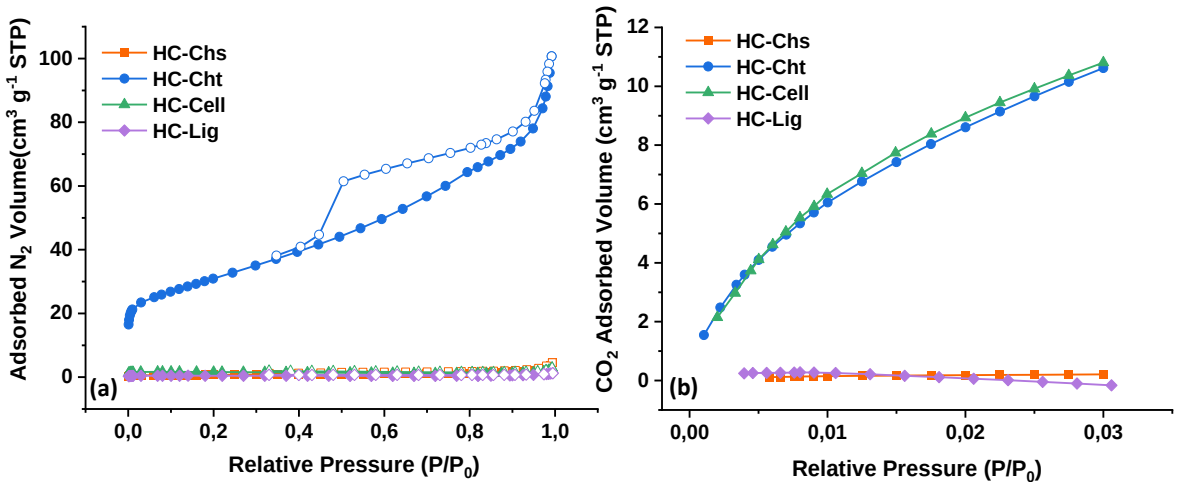

Figure 3: (a) Nitrogen adsorption/desorption isotherms measured at 77 K and (b) CO_2 adsorption isotherms measured at 273 K of HC materials: HC-Chs, HC-Cht, HC-Cell and HC-Lig.

Surprisingly, HC-Cht presents a type IV isotherm with an H1 hysteresis loop characteristic for micro- and mesoporous materials. The S_{BET} of this material is significantly higher (110 $m^2\ g^{-1}$) than for the other HCs (<10 $m^2\ g^{-1}$). Such a high surface area could be developed during some *in situ* activation reactions, described in detail in our previous work, [41] occurring between the carbon structure and the Ca-based impurities. Complementary CO_2 adsorption was also performed (Figure 3b) to detect the presence of ultramicropores (<0.7 nm) which might exist and might not be accessible to N_2 gas. [11] We have previously demonstrated [36] that a lower SSA_{CO2} leads to a lower iCE. In the present case, the HC-Chs and HC-Lig adsorb a very low amount of CO_2 volume (close to 0) and their S_{BET} CO_2 (<1 $m^2\ g^{-1}$) is also low. On the contrary, HC-Cht and HC-Cell adsorb a much higher amount of CO_2 volume and have a higher S_{BET} (72–74 $m^2\ g^{-1}$).

The surface chemical composition analyzed by XPS (Table 2) displays high C contents for HC-Cht and HC-Cell (96.22 and 95.61 at. %) and much lower content of C for HC-Lig and HC-Chs (83.91 and 78.93 at. %). For the latter materials, the O content is rather high (11.81 at. % and 14.88 at. %) as compared to the values for HC-Cht and HC-Cell (2.84 at. % and 3.38 at. %).

The high amount of oxygen can be explained by the presence of impurities: Na (2.78 at. %) and K (0.79 at. %) for HC-Lig and Ca (4.33 at. %) and Na (0.68 at. %) for HC-Chs, respectively, corresponding to carbonates, sulfides, and/or sulfates detected by XRD. A small amount of N (0.71 at. %) and S (0.36 at. %) was found, respectively, for HC-Chs and HC-Lig. Most probably it is a "fingerprint" of their parent precursor composition (Table S1, Supporting Information). For HC-Cht and HC-Cell, a small amount of, respectively, Ca (0.95 at%) and Si (1.02 at. %) was detected.

Further understanding of the bulk chemical functionalities was gained by TPD-MS analysis. First, the type of functional group was determined. During a typical experiment, the HC oxygen-functional groups are thermally degraded with the release of CO and CO_2 gases. Typical gas desorption profiles as a function of the heating temperature are illustrated in Figure 4. For CO_2 desorption (Figure 4a), several peaks are observed within a broad temperature range. At low temperatures (<500 °C), the CO_2 groups are generated by the decomposition of carboxyl (−COOH), anhydride (−COO-OR), and lactone (−COO−) functional groups. Their corresponding peaks are rather broad and low in intensity, indicating a small amount of these groups. Very sharp peaks appear at ∼500 °C for HC-Cht and at ∼550 °C for HC-Chs and HC-Lig. For the latter carbon, there is also a second peak at ∼670 °C. The presence of CO_2 peaks at high temperatures (>500 °C) can be associated with the decomposition of carbonate-based impurities. [49, 50] This has already been observed in our previous studies [8, 41, 42] and correlated to the disappearance of the CO_2 peak upon the removal of carbonates by HCl and/or water washing.

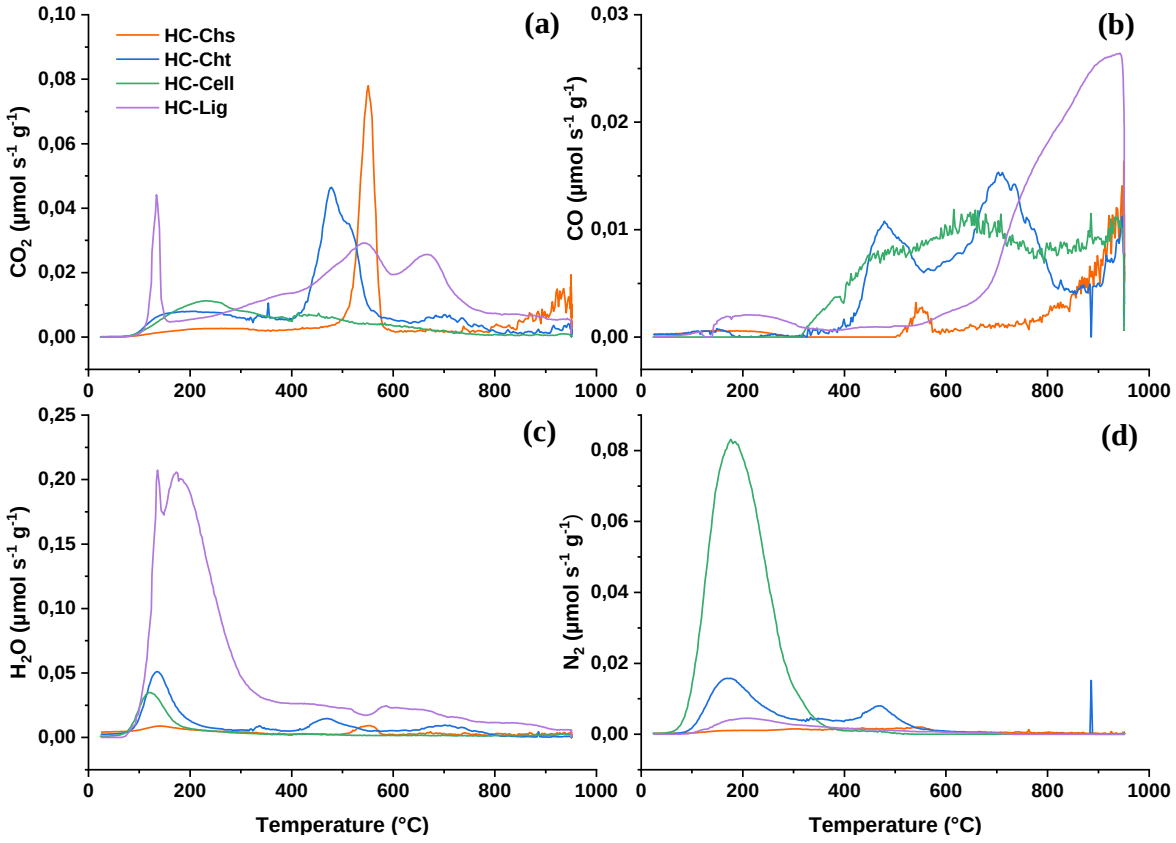

Figure 4: Gas desorption profiles of (a) CO_2, (b) CO, (c) H_2O and (d) N_2 obtained by TPD-MS for HC-Chs, HC-Cht, HC-Cell and HC-Lig hard carbons.

Moreover, for HC-Lig, a sharp CO_2 peak seen at ~130 °C is accompanied by a sharp H_2O peak (Figure 4b). A second broad and intense H_2O peak appears at ~175 °C. This relatively high temperature of water release suggests instead a chemisorbed water, probably in sodium carbonate phases. Low S_{BET} N_2 and CO_2 (Table 2) determined for this material allow us to exclude the presence of physisorbed water and support the chemisorbed water hypothesis. On the contrary, for HC-Cht and HC-Cell, the presence of a physisorbed water (~130 °C) can be observed, yet its amount is rather negligible. These two materials present either high S_{BET} N_2 (110 m^2 g^{-1}, HC-Cht) or/and high S_{BET} CO_2 (72 m^2 g^{-1} for HC-Cht and 74 m^2 g^{-1} for HC-Cell). They also release a significant amount of N_2 (Figure 4d) trapped in the very narrow pores or present in their composition. Finally, no water or N_2 peak is observed for HC-Chs which has a very low S_{BET} N_2 and CO_2 (<2.5 m^2 g^{-1}).

Other functional groups such as phenol (C–OH), ether (C–O–R), and quinone (C═O), if present, typically leave the surface of carbon between 400 and 950 °C as CO gas (Figure 4b). HC-Chs shows a low release of CO while HC-Cht exhibits two peaks around 500 and 700 °C. The first CO peak can be related to the presence of anhydrides which leave the surface of the carbon at almost the same time as CO_2-containing groups. The second peak can be ascribed to the decomposition of phenols. We also observe a very strong contribution of CO groups in HC-Cell, which might be related to several oxygen-based groups (anhydrides, phenols, and ethers). As for the HC-Lig, there is only one well-defined and intense peak between 600 and 905 °C probably due to the presence of more thermally stable functional groups, i.e., ethers and quinones.

The amount of CO and CO_2 and their total amount, CO_x, is presented in Figure 5a. In general, for all the studied materials except one, HC-Cell, the amount of CO_2 groups is higher than that of CO groups, which is a consequence of the presence of carbonates whose thermal decomposition is accompanied by the release of CO_2. The total amount of CO_x groups varies in the following order: HC-Lig > HC-Cht > HC-Cell, and HC-Chs

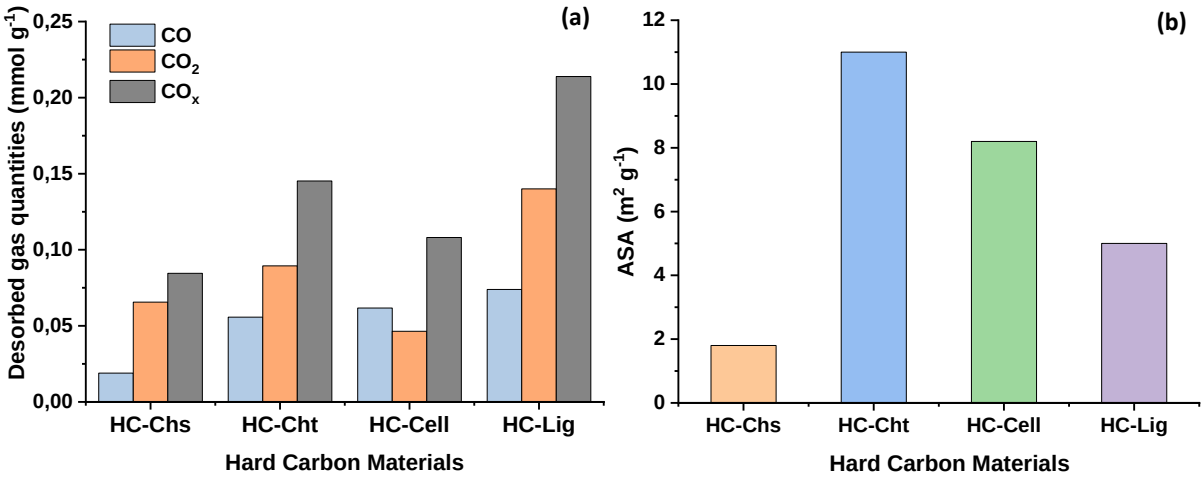

Figure 5: (a) Desorbed amounts of CO, CO_2 and CO_x (CO + CO_2) gases released by thermal decomposition during the TPD-MS experiment and (b) the active surface area (ASA) of hard carbon materials.

The same technique, TPD-MS, was used to assess the active surface area of HCs, namely, the surface containing carbon defects. The impact of defects on Na-storage is not fully understood, but several studies point out its pivotal role in the adsorption of Na ions. [51-53] Bommier et al. [12] reported a linear relationship between the defects determined qualitatively by Raman spectroscopy (I_D/I_G ratio), while our group [11] confirmed this relationship quantitatively based on the active surface area and the specific capacity obtained in the slope region of the galvanostatic charge/discharge curve. Both publications mentioned a decrease of slope-region specific capacity with the decrease in carbon defects. Therefore, the quantification of defects remains essential.

To determine the active surface area (ASA) of HC, the material is exposed to O_2 chemisorption at 300 °C once the first TPD-MS analysis has finished. This step allows the active sites (edge defects, vacancies, and so forth) to absorb O_2 and to form other oxygen-functional groups which are further quantified to calculate the ASA. The CO and CO_2 gas desorption profiles of the newly formed functional groups are different (Figure S4, Supporting Information), indicating various amounts and types of active sites existing in HCs. It can be seen in Figure 5d that the ASA values differ depending on the parent material used to prepare the HC. The lowest value (1.8 $m^2\ g^{-1}$) is obtained for HC-Chs. It can be explained by the high degree of structural ordering represented by the presence of graphitic regions, low d_{002} (3.65 Å), and low S_{BET} (<2.5 $m^2\ g^{-1}$). HC-Cht, despite the smallest d_{002} (3.60 Å), has the highest ASA (11 $m^2\ g^{-1}$) which can be associated with high N_2 (110 $m^2\ g^{-1}$) and $CO_2 S_{BET}$ (72 $m^2\ g^{-1}$). HC-Cell also presents a high ASA (8.8 $m^2\ g^{-1}$) most probably related to the presence of ultramicropores (S_{BET} CO_2 = 74 $m^2\ g^{-1}$) and its higher disorder degree emphasized by larger d_{002} (3.81 Å) and higher I_D/I_G ratio. Finally, HC-Lig exhibits an intermediate ASA (5.0 $m^2\ g^{-1}$) compared to the rest of the studied carbons. The ASA values presented in here are in good agreement with those reported for other carbons. [5]

To sum up, despite being synthesized in similar conditions, the HCs obtained from cellulose, chitin, chitosan, and lignin are not alike. The parent material plays a crucial role in governing the physicochemical properties of the hard carbon. It strongly influences its structure, surface chemistry, porosity, and its morphology, and, thus, the electrochemical performance of the HC and its interactions with the electrolyte.

3.2 Electrochemical Characterisation

3.2.1 Electrochemical performance without carbon additive

The impact of two parameters is discussed in this subsection: (i) the choice of the binder (and the corresponding solvent used for its dissolution) and (ii) the carbon additive impact. Water-based CMC and NMP-based PVDF binders were used to assess the electrochemical performance of HC in 1 M $NaPF_6$/EC:DEC electrolyte without carbon black additive. The comparison of the specific charge capacity and Coulombic efficiency delivered by the four studied HCs during cycling (at C/10 rate for the two formation cycles and C/5 for the following cycles) is shown in Figure 6a,b and Table 3. Different cycling behavior was observed depending on the binder used for the electrode formulation. When PVDF binder was used, the specific capacities were similar for most of the carbons (~221–226 mAh g^{-1}), except for HC-Cell which delivered more than 300 mAh g^{-1} (315 mAh g^{-1}). When CMC binder is employed, HC-Cht and HC-Cell show higher values (between 243–283 mAh g^{-1}) than for PVDF, whereas for HC-Chs and HC-Lig, the values are two times lower (90–126 mAh g^{-1}).

Those results indicate that the electrochemical performance is significantly affected by the presence of impurities and their interaction with the solvent used for the electrode formulation. Carbonates are most likely to be dissolved during the electrode fabrication, then by polluting the ink. It has been shown that such impurities decrease the material's electronic conductivity and contribute to SEI formation and can interact with the counter electrode, if they dissolved

during the electrochemical process. [8, 23] Indeed, the electronic conductivity of HC-Cht powder, determined according to the general procedure described in SI, is much lower (14.3 S/cm) than that of HC-Cht (19.5 S/cm). For the two others materials, HC-Cell and HC-Cht, as the impurities have a limited role, the physicochemical parameters do have an impact. The precise reason for such a tendency is difficult to provide considering the complex and controversial Na-ion insertion mechanisms into HCs. [11, 12, 14, 44, 54-56] However, the insertion of Na^+ is considered to occur on the carbon surface (defects/porosity), between the graphene layers and/or into the closed pores.

Based on the physicochemical properties, the HC-Cell was expected to outperform the other HCs owing to its large interlayer space which is favorable for Na^+-ion insertion, high purity, and small surface area that should limit the electrolyte decomposition, whereas the HC-Cht was thought to be the weak link in the series of the studied HCs mainly due to its high specific surface area. Impurities detected on HC-Lig and HC-Chs were expected as well to affect in particular the iCE and the overall cycling behavior. [8, 41, 42]

As for the capacity fading, there are some important differences too. The carbon-based electrodes formulated with CMC binder achieve stable capacity after only a couple of cycles and are able to maintain it up to 50 cycles. The electrodes formulated with PVDF require at least 20 cycles to stabilize their capacity. In both cases, the capacity fading is most probably related to the SEI formation and/or irreversible trapping of Na-ions in the HC structure. [57] The SEI formation influences also the initial Coulombic efficiency as can be seen in Table 3.

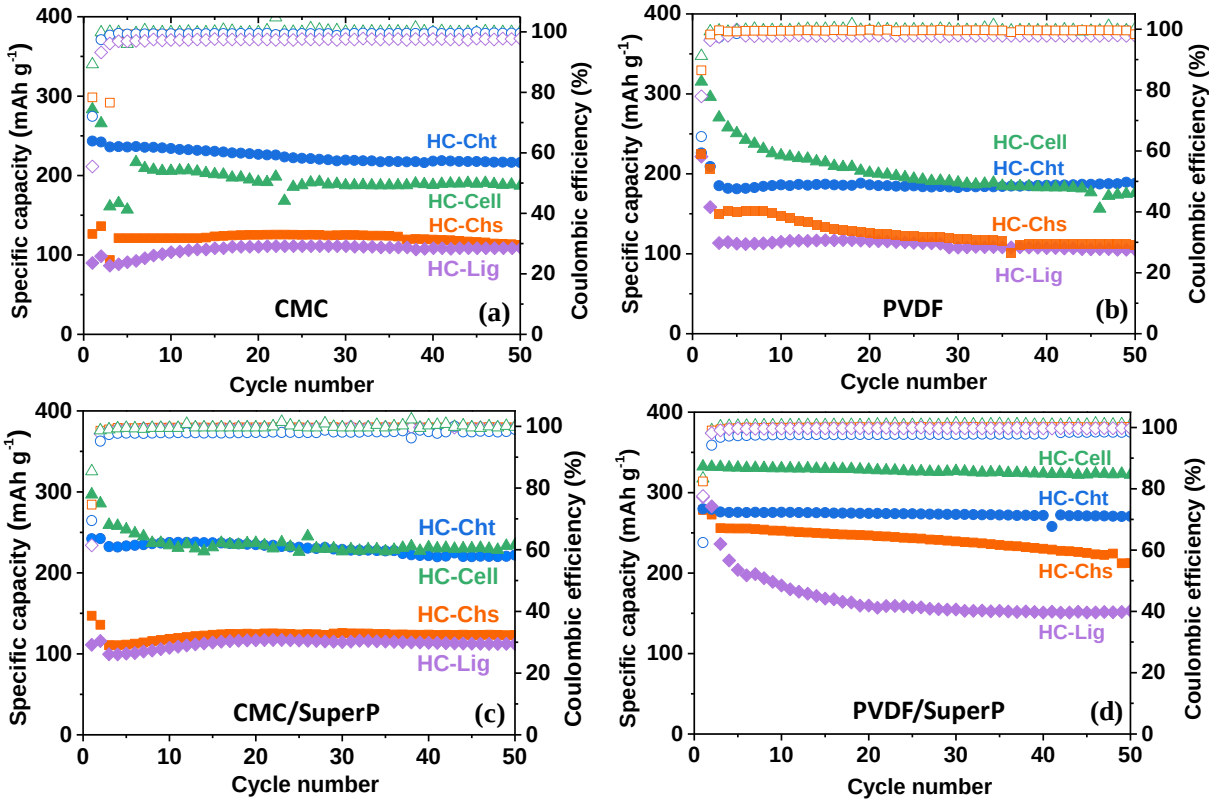

Figure 6: Specific charge capacity (full symbols) and Coulombic efficiency (empty symbols) of the Na-ion half-cells tested with electrodes based on four different HCs formulated with (a) CMC, (b) PVDF (c) CMC /Super P and (d) PVDF/SuperP binders in 1 M $NaPF_6$ in EC:DEC electrolyte. The first two cycles were performed at a rate of C/10. The rest of the cycling proceeded at a rate of C/5.

The physicochemical properties can explain further some of the observed tendencies. HC-Cell achieves the highest iCE regardless of the binder used in the electrode formulation (91% PVDF vs 89% CMC) which might be linked to the low level of inorganic impurities. HC-Lig shows some variations in iCEs as a function of the electrode‘s binder (ca. 55% for CMC vs. 78% for PVDF) which cannot be attributed to the carbon itself but rather to the presence of impurities that appears to be a dominant factor, similarly to the case of HC-Chs (Table 3).

Table 3. Initial Coulombic efficiency (iCE), first charge capacity (1st Cch) and capacity retention after 50 cycles (Cret) obtained for all four HC-based electrodes depending of the binder used.

Binder	**PVDF**			**CMC**		
Materials	**iCE %**	**1st Cch mAh g^{-1}**	**Cret %**	**iCE %**	**1st Cch mAh g^{-1}**	**Cret %**
HC-Chs	87 (82)	224 (278)	49 (76)	78 (75)	126 (147)	90 (84)
HC-Cht	65 (62)	226 (280)	80 (97)	72 (70)	243 (242)	89 (92)
HC-Cell	91 (83)	315 (332)	62 (97)	89 (85)	283 (297)	66 (79)
HC-Lig	78 (78)	221 (294)	48 (52)	55 (61)	90 (111)	120 (100)

The values reported in the brackets refer to the electrochemical performance of the electrodes containing carbon black.

3.2.2 Electrochemical performance with carbon additive

When carbon black is added during the electrode formulation (Figure 6c,d), the iCE slightly decreases for most of the materials due to the SEI being created at the carbon additive surface owing to its high surface area (60 m^2 g^{-1}) and high intergrain porosity induced by its nanometer size. [54]

Regarding the specific capacity, two different trends can be distinguished depending on the electrode's formulation. For the CMC-based electrodes, there is almost no difference in specific capacity gained with or without SuperP (Table 3), indicating that the electrochemical performance of these type of electrodes is not related to the lack of electronic conductivity but rather to the surface, structure, and the porosity of the HC, as well as to the presence of impurities. For the PVDF-containing electrodes, the addition of carbon black leads to a significant increase in the specific capacity regardless of the HC used. HC-Cell delivers the highest specific capacity (ca. 332 mAh g^{-1}), followed by HC-Lig (ca. 294 mAh g^{-1}), HC-Cht

(ca. 280 mAh g^{-1}), and finally HC-Chs (ca. 278 mAh g^{-1}). For the HC-Cell and HC-Cht, the higher purity of the active material is directly reflected in a very high and stable specific capacity, also preserved during long-term cycling. For HC-Chs and HC-Lig, the specific capacity is lower and seems to fade quicker, most probably due to the presence of impurities. [42] Additionally, as demonstrated by TDP-MS, HC-Lig contains a significant amount which can be released into the electrolyte enhancing the capacity fading and the degradation of the entire electrochemical system.

Indeed, for HC-Lig during the first 5 cycles there is a rapid capacity decay from 292 mAh g^{-1} for the first cycle to 204 mAh g^{-1} for the fifth cycle. This decay is followed by a less severe capacity decrease between the fifth and the 20th cycle, and finally by its stabilization at around ~150 mAh g^{-1}. On the contrary, for the HC-Cell and HC-Cht, the specific capacity seems stable during cycling, and a high-capacity retention of 97% is preserved after 50 cycles (Table 3).

The choice of the electrode's binder not only dictates the overall electrochemical performance of the HCs but also induces changes in the reaction mechanism, which can be deducted from the analysis of the galvanostatic curves. The first charge/discharge curve of the HC-Cht and HC-Cell formulated with CMC and PVDF (Figure 7a) is characterized by a sloping region in the high potential range (>0.1 V) and a potential plateau region in the low potential range (<0.1 V). The presence of these two regions is not related to the binder used in the electrode formulation but specifically to the HC physicochemical properties.

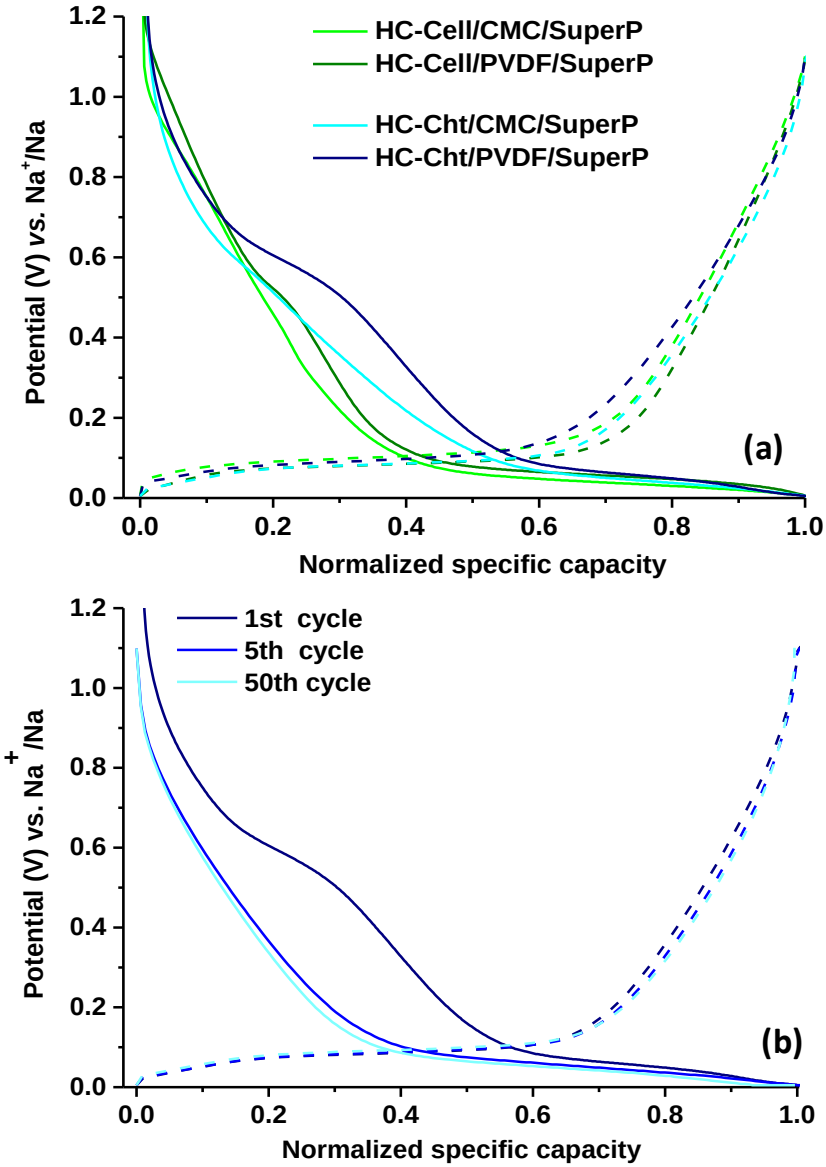

Figure 7: (a) 1st charge/discharge cycle for the cells assembled with HC-Cell and HC-Cht formulated with CMC /SuperP and PVDF /SuperP, and (b) the charge/discharge profiles of the 1st, 5th and 20th cycle for the HC-Cht PVDF/SuperP. These tests were performed using in 1 M $NaPF_6$ in EC:DEC as electrolyte.

For HC-Cell, the specific capacity gained within a slope potential region is lower than that obtained within the plateau region (40% vs 60% of the entire capacity, respectively). Interestingly, the opposite trend is observed for the HC-Cht, as 60% of the capacity is gained within a slope potential region while 40% of it is attained within the plateau. Additionally, one can notice a kind of "bump" being present below 0.6 V, which seems to be binder-dependent

as it appears only for the cells assembled with PVDF-based electrodes. This "bump" is thought to be related to the PVDF decomposition and/or SEI formation because it is no longer visible in the curves corresponding to the 5^{th} and 50^{th} cycle (Figure 7b). Furthermore, the interactions between the electrolyte and the binder might also vary between water-based and organic solvent-based systems, as suggested by the results of the contact angle measurements (Figure S5, Supporting Information).

To better understand this latter hypothesis, one should be reminiscent of the physicochemical properties of the chitin- and cellulose-derived hard carbons. The former of the two, HC-Cht, has a very high specific surface area that should promote Na-ion adsorption and SEI formation. In addition, it is characterized by lower *d*-spacing, which is not very favorable for the Na insertion in between the graphene layers. All properties combined lead to a broad slope potential region mentioned previously. Unlike HC-Cht, HC-Cell should enhance the Na insertion in between the graphene layers owing to its Na-ion favorable *d*-spacing, which, in turn, should result in a longer low potential plateau, translating into a more specific capacity. This is well illustrated in the cycles succeeding the first cycle, for example, cycles 5 and 20 (Figure 7b and Figure S6, Supporting Information), for which the obtained specific capacity comes mostly from the potential plateau region and not from the slope potential region.

The impact of the choice of the electrolyte, more precisely the sodium salt ($NaPF_6$ vs $NaClO_4$), on the electrochemical performance of the HC materials exhibiting the lowest overall specific capacity and capacity retention (HC-Chs and HC-Lig) was studied for the PVDF-based electrodes. As can be seen in Figure 8 and Table 4, the iCE and the specific capacities were rather similar, regardless of the electrolyte salt used in the electrolyte. As for the capacity retention, an improvement was only observed for HC-Lig (an increase from 52% ($NaPF_6$) to 70% ($NaClO_4$)) whereas for HC-Chs the retained capacity remained almost unchanged (70–76%).

The charge/discharge profiles for the first, fifth, and 20th cycles are shown in Figure S7d (Supporting Information). During the first cycle, a pseudoplateau at 0.5 V corresponding to SEI formation is observed for both HCs in the presence of $NaClO_4$, yet it is more pronounced for HC-Lig (Figure S6d). This might suggest that the SEI layer is thicker and/or has a different composition. When $NaPF_6$ is used as electrolyte salt, the formation of the SEI in the case of HC-Lig seems to start at a potential lower than 0.5 V (Figure S7b), which might explain the difference in capacity retention. For further cycles (5th and 20th), the galvanostatic curves are overlapping, pointing to a good reversibility of the reactions.

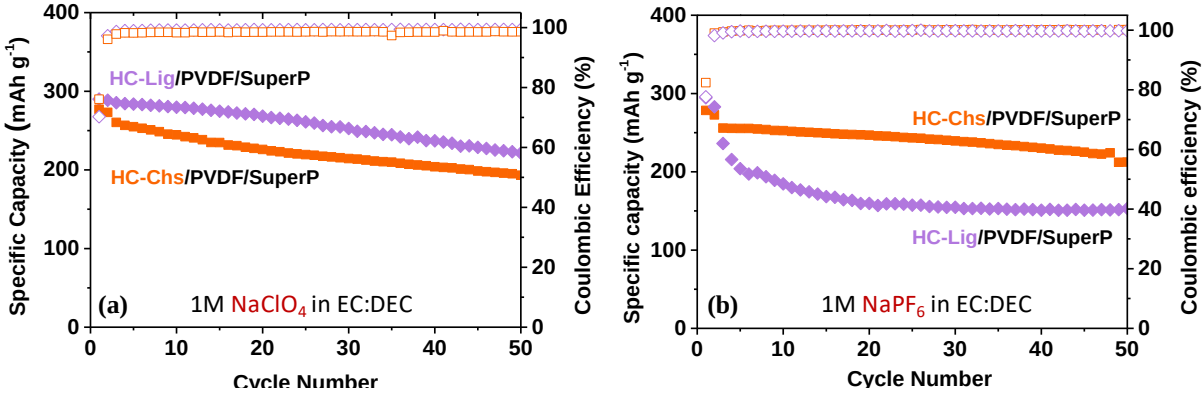

Figure 8: Specific capacity (full symbols) and Coulombic efficiency (empty symbols) of the Na-ion half-cells tested with electrodes based on HC-Lig and HC-Chs formulated with PVDF /SuperP, and (a) 1M $NaClO_4$ in EC:DEC and (b) in 1M $NaPF_6$ in EC:DEC.

Table 4: Initial coulombic efficiency (iCE), first charge capacity (1^{st} Cch) and capacity retention after 50 cycles (Cret) obtained for HC-Chs and HC-Lig formulated with PVDF and Super P, tested in two different electrolytes: 1M $NaClO_4$ and 1M $NaPF_6$ in EC: DEC.

Electrolyte				**$NaClO_4$**		
Materials	**iCE %**	**1^{st} Cch mAh g^{-1}**	**Cret %**	**iCE %**	**1^{st} Cch mAh g^{-1}**	**Cret %**
HC-Chs/PVDF/SuperP	76	277	70	82	278	76
HC-Lig/PVDF/SuperP	70	290	76	78	294	52

3.3 Discussion

We have seen that the electrode formulation (the choice of binder and the absence/presence of carbon black additive) has an impact on the iCE and specific capacity of the HCs. However, as usual, it is difficult to determine a clear structure–electrode formulation–performance correlation due to a considerable number of parameters that influence the overall electrochemical performance. Nevertheless, we tried to establish some links based on the collected data, which are summarized below:

- The iCE seems to be directly related to the specific surface area of the HC, and the amount of the oxygen-based functional groups, impurities, and the presence of carbon defects (Figure 9), all of which trigger the electrolyte decomposition. Moreover, regardless of the electrode formulation, the iCE is generally higher for the hard carbons having SSA N_2 < 10 m^2 g^{-1}, here HC-Cell and HC-Chs, (Figure 9a), with the exception for HC-Lig which does not follow this tendency despite its small SSA. This might be associated with the significant level of impurities present in this material (Figure 9b). The SSA N_2 > 10 m^2 g^{-1}, as for example in the case of HC-Cht, usually goes hand-in-hand with lower iCE.
- The impurities undoubtedly play a crucial role in defining the electrochemical performance of the hard carbon and may as well affect the Coulombic efficiency attained at the beginning of cycling (Figure 9b). As an example, HC-Cht and HC-Lig show the lowest iCE among the studied HCs despite a slightly different impurity content (∼4 at. % vs ∼16 at. %, respectively). In the case of HC-Cht, low iCE might be a result of not only the presence of impurities but also of its high SSA N_2, notably the highest SSA of the HCs tested.
- The surface functional groups have also their share in defining the iCE. If we consider the COx groups, derived from the decomposition of oxygen-based functional groups and metal carbonate impurities (Figure 9c), one can notice that HC-Cht and HC-Lig, having the

highest amount of COx, are characterized by the lowest iCE, whereas HC-Cell and HC-Chs, containing much less of the COx groups, achieve higher iEC.

- Last but not least is the active surface area, ASA, which plays an important role. It can be seen that the iCE generally decreases while the ASA/SSA CO_2 ratio increases (Figure 9d). Once again, HC-Cht is off the trend as it presents a different porosity. Besides ultramicropores (detected by CO_2), it also contains micro- and mesopores (detected by N_2 adsorption), all of which impact the iCE.

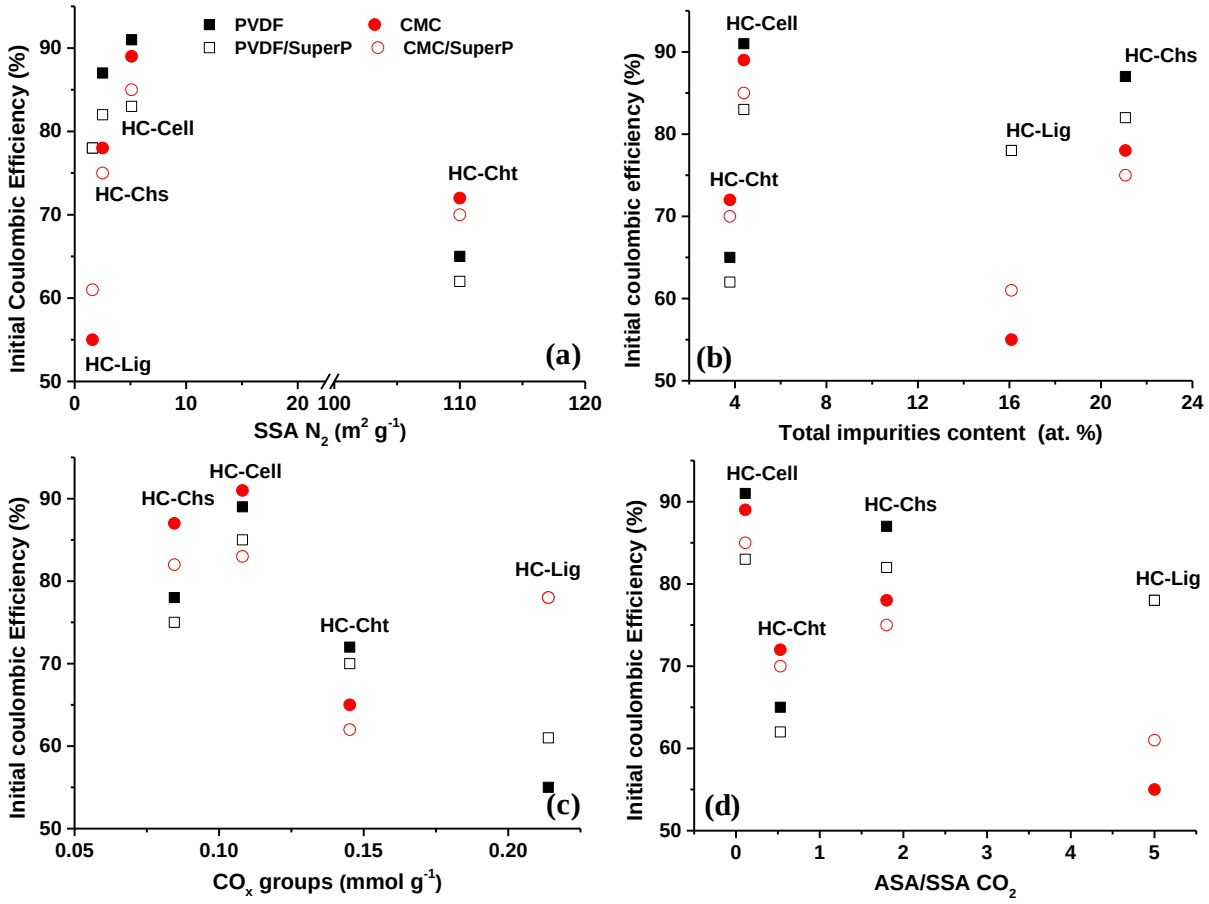

Figure 9: Correlation between the initial coulombic efficiency, iEC, and (a) the specific surface area, SSA N_2, (b) the level of impurities (including inorganic impurities, oxygen- and other heteroatom-containing impurities detected by XPS), c) the oxygen-containing functional groups, COx and (d) the ratio of ASA to SSA CO_2 for all four hard carbons formulated with PVDF and CMC binders without and with SuperP, and tested in 1M $NaPF_6$ in EC:DEC.

The electrochemical performance of the HC is also highly dependent on the electrode formulation, the choice of binder, and the absence/presence of the carbon additive. Some key findings concerning this part of the study are presented in Figure 10 and can be summarized as follows:

- The presence of carbon additive typically induces from 2% to 8% lower iCE, which is slightly more pronounced for the PVDF-based formulations (3–8%) than for those containing CMC (2–6%).
- For the binder, the impact on iCE is seen for CMC (24–34%) more than for PVDF (21–26%).
- For the active material, the formulation induces 8% to 23% of differences in the iCE, i.e., 8% and 10% for "pure" hard carbons (HC-Cell and HC-Cht, respectively), and 12% and 23% for HCs rich in impurities (HC-Chs and HC-Lig, respectively).

Moreover, the amount of carbon in the HC is an important parameter too. It may increase the obtained specific capacity (Figure 10a). The HCs rich in carbon (HC-Cell and HC-Cht) provide the highest specific capacity, regardless of the chosen binder and the presence of conductive additive. Those with a low amount of carbon (HC-Lig and HC-Chs) do not perform well. In addition, they often contain a considerable amount of inorganic and oxygen-containing impurities, further reducing the amount of sites available for Na-insertion (Figure 10b), which is especially pronounced in the presence of the CMC binder. Moreover, because the insertion of Na-ions occurs mainly in between the graphene layers, the distance between these layers, expressed as the *d*-spacing, also affects the attained specific capacity (Figure 10c). An increase in the specific capacity is often dictated by the enlargement of d_{002}. HC-Cell which has the highest d_{002} delivers the best capacity, while HC-Cht has the lowest, for a formulation made of PVDF–SuperP.

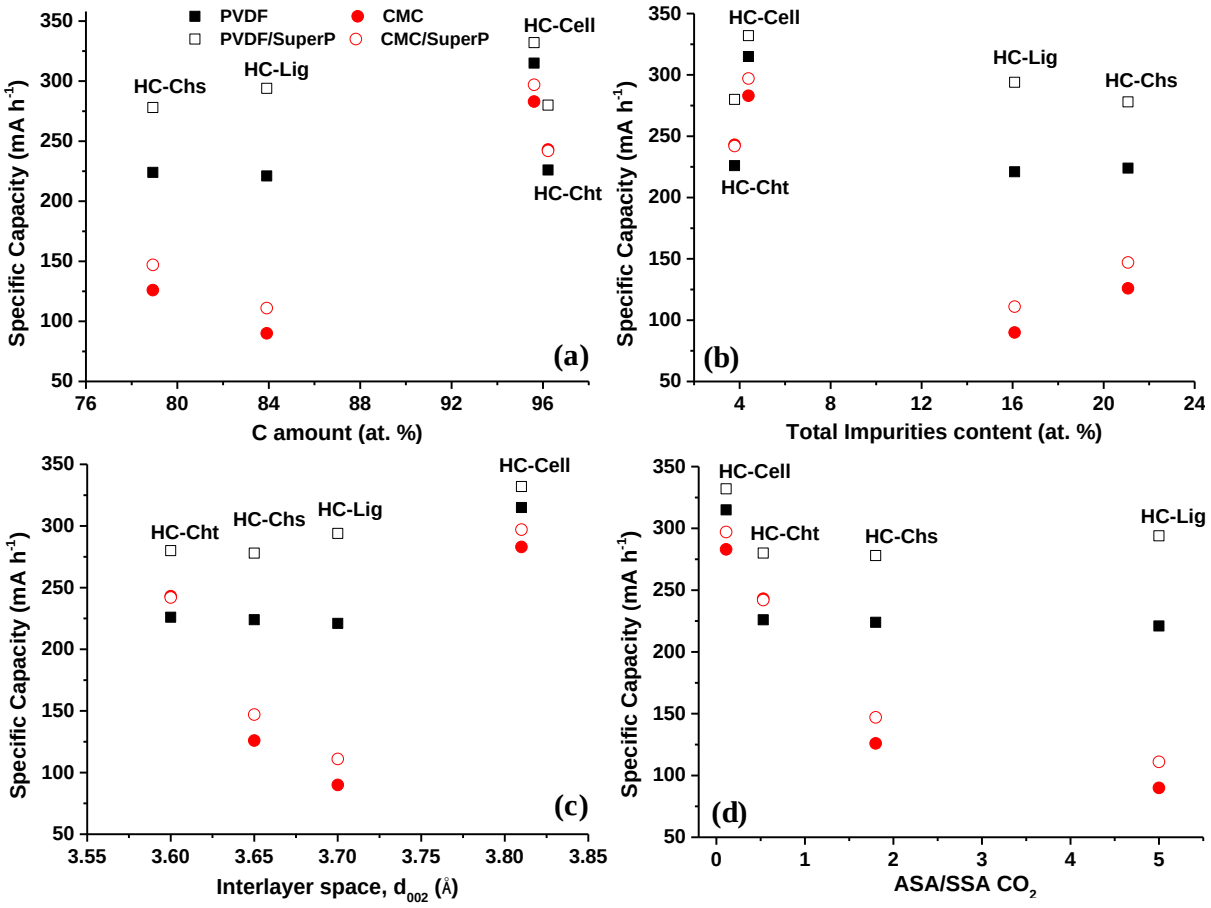

Figure 10: Correlation between the specific capacity and (a) the carbon amount (b) the level of impurities (including inorganic impurities, and oxygen- and other heteroatom-containing impurities detercted by XPS), c) the interlayer spacing, d_{002}, and (d) the ratio of ASA to SSA CO_2. for all four hard carbons formulated with PVDF and CMC binders without and with SuperP and tested in 1M $NaPF_6$ in EC:DEC.

For HC-Chs and HC-Lig, the correlations are very scattered and strongly dependent on the used formulations, meaning that the electrochemical performance–electrode formulation correlation is not very obvious. One of the reasons might be the high level of impurities in HC impeding Na-insertion. Moreover, a high ASA to SSA CO_2 ratio (the number of the edge defects normalized to the surface of the carbon) leads to a decrease in specific capacity as well (the case of HC-Lig, Figure 10d).

For all studied hard carbons, the electrode formulations with PVDF binder bring a higher specific capacity; at the same time, the presence of carbon additive, SuperP, has a positive effect on both formulations, with CMC and PVDF polymers, further confirming a poor electronic conductivity of the active material. Moreover, depending on the formulation, the difference in the attained specific capacity for the purest hard carbons seems negligible (49 and 54 mA h g^{-1}, respectively, for HC-Cell and HC-Cht), while that for the HCs rich in inorganic and oxygen-containing groups exceeds 50 mAh g^{-1} (152 and 204 mAh g^{-1}, respectively, for HC-Chs and HC-Lig). For these electroactive materials, the PVDF–SuperP combination provides the highest specific capacities, further supporting the hypothesis of the lack of sufficient electronic conductivity. The water-based electrodes prepared with the CMC binder deliver the lowest specific capacities, which can be associated with the high content of impurities in the HC mentioned before, inducing low electronic conductivity, due to some possible dissolution of impurities into the electrolyte and specific interactions of the impurities with the binder and/or the current collector. As a result, the attained specific capacity is strongly related to both the intrinsic properties of hard carbon and the applied electrode formulation. It should be noted that when the carbon material is of high purity (HC-Cell), high performance is obtained for the CMC electrodes (∼297 mAh g^{-1}). Although the capacity is slightly lower than the PVDF counterpart (332 mAh g^{-1}) and that the stability during first cycles must still be improved, the advantages of the CMC-water formulation (renewable, nontoxic, easily degradable, and recyclable) make it appealing from an environmental and industrial application point of view.

CONCLUSIONS

The impact of the electrode formulation and the choice of the electrolyte on the electrochemical performance of four hard carbons was investigated in Na half-cells. It was found that distinct biopolymers lead to HC materials with different physicochemical properties, in terms of structure, porosity, surface chemistry/defects, and morphology. Among the carbonaceous

materials studied, cellulose-derived HC showed the largest interlayer spacing and the lowest level of impurities. The HCs obtained from chitosan and lignin contained a relatively high level of inorganic impurities, mainly based on Na and Ca. Finally, HC derived from chitin was found to be off-trend, with its high specific surface area and mesoporous texture.

We demonstrated that, in the absence of a conductive additive, SuperP, the HCs behave differently depending on the binder used to formulate the electrodes. Rather similar electrochemical performance was obtained for all hard carbon-based electrodes prepared with PVDF binder, while for the electrodes formulated with CMC polymer, we have observed some differences (for example, almost two times lower specific capacity for HC-Lig and HC-Chs), which in the case of HC-Lig was assigned to the presence of inorganic impurities.

In the presence of SuperP, a slight decrease in iCE was observed for all studied hard carbons and electrode formulations; however, the specific capacity was improved, in particular very significantly, for PVDF formulations. The latter enhancement was associated with the improvement in the electronic conductivity of the electrode material. The differences in the capacities of the electrodes obtained with CMC or PVDF binders (with or without SuperP) are very important for HC materials having impurities. Indeed, a significant effect of the HC properties on its electrochemical performance has been highlighted. Electroactive materials rich in carbon, with a low level of impurities, low oxygen content, and large interlayer spacing, delivered the highest specific capacity, i.e., HC-Cell (332 mAh g^{-1}), followed by HC-Cht and HC-Chs (~280 mAh g^{-1}). HC-Lig with its high level of impurities struggled to cycle properly and to deliver a decent specific capacity (severe capacity fading over cycling). This drawback could be overcome by using a $NaClO_4$-based electrolyte, allowing an increase in the capacity retention after 50 cycles to 76%, instead of 52% when using $NaPF_6$. However, no impact of the electrolyte salt on iCE or the specific capacity was observed.

To sum up, the anode formulation providing the highest performance was obtained with HC having high purity, low porosity, and large interlayer space, with carbon black as additive and PVDF as binder. Therefore, a careful electrode engineering (including the choice binder and the addition of carbon black) combined with a proper electrolyte selection and tuning of the HC properties is the only means for achieving a high specific capacity (332 mAh g^{-1}) and high retention over 50 cycles (97%).

SUPPORTING INFORMATION

TGA and TGA derivative curves of biopolymer precursors, elementary chemical analyses of biopolymer precursors, SEM images of hard carbon materials, Raman spectra of hard carbons, TPD-MS gas desorption profiles of hard carbons after the oxygen chemisorption step, electrical conductivity measurement experimental procedure, contact angle measurements on hard carbon electrode, charge/discharge profiles of HC-Cht and HC-Cell, charge/discharge profiles of HC-Chs and HC-Lig,

ACKNOWLEDGMENTS

The authors acknowledge G. Schrodj, B. Réty, and Dr. J. Dentzer for TGA and TPD-MS experimental and data analysis support. We thank as well Dr. L. Vidal and Dr. Ph. Fioux for the help provided with the TEM and XPS analyses done through IS2M technical platforms. This work was performed in the frame of RS2E (French research network on electrochemical energy storage) and financially supported by European Union's Horizon 2020 Program (Project NAIADES, Call LCE10-2014, Contract No. 646433).

REFERENCES

1. Xie, F.; Xu, Z.; Guo, Z.; Titirici, M., Hard carbons for sodium-ion batteries and beyond. *Progress in Energy* **2020,** *2*, 042002.

2. Irisarri, E.; Ponrouch, A.; Palacin, M. R., Review—Hard Carbon Negative Electrode Materials for Sodium-Ion Batteries. *Journal of The Electrochemical Society* **2015,** *162* (14), A2476-A2482.

3. Xiao, B.; Rojo, T.; Li, X., Hard Carbon as Sodium-Ion Battery Anodes: Progress and Challenges. *ChemSusChem* **2019,** *12* (1), 133-144.

4. Tarascon, J.-M.; Armand, M., Issues and challenges facing rechargeable lithium batteries. *Nature* **2001,** *414*, 359-367.

5. del Mar Saavedra Rios, C.; Beda, A.; Simonin, L.; Matei Ghimbeu, C., *Hard Carbon for Na-ion Batteries: From Synthesis to Performance and Storage Mechanism. In Na-ion Batteries (eds L. Monconduit and L. Croguennec).* ISTE Ltd 2020. Published by ISTE Ltd and John Wiley & Sons, Inc.: 2021.

6. Jin, Q. Z.; Wang, K. L.; Feng, P. Y.; Zhang, Z. C.; Cheng, S. J.; Jiang, K., Surface-dominated storage of heteroatoms-doping hard carbon for sodium-ion batteries. *Energy Storage Materials* **2020,** *27*, 43-50.

7. Daher, N.; Huo, D.; Davoisne, C.; Meunier, P.; Janot, R., Impact of Preoxidation Treatments on Performances of Pitch-Based Hard Carbons for Sodium-Ion Batteries. *Acs Applied Energy Materials* **2020,** *3* (7), 6501-6510.

8. Beda, A.; Le Meins, J. M.; Taberna, P. L.; Simon, P.; Ghimbeu, C. M., Impact of biomass inorganic impurities on hard carbon properties and performance in Na-ion batteries. *Sustainable Materials and Technologies* **2020,** *26*, e00227.

9. Hong, Z.; Zhen, Y.; Ruan, Y.; Kang, M.; Zhou, K.; Zhang, J.-M.; Huang, Z.; Wei, M., Rational Design and General Synthesis of S-Doped Hard Carbon with Tunable Doping Sites toward Excellent Na-Ion Storage Performance. *Advanced Materials* **2018,** *30* (29), 1802035.

10. Xiang, J.; Lv, W.; Mu, C.; Zhao, J.; Wang, B., Activated hard carbon from orange peel for lithium/sodium ion battery anode with long cycle life. *Journal of Alloys and Compounds* **2017,** *701*, 870-874.

11. Matei Ghimbeu, C.; Górka, J.; Simone, V.; Simonin, L.; Martinet, S.; Vix-Guterl, C., Insights on the Na+ ion storage mechanism in hard carbon: Discrimination between the porosity, surface functional groups and defects. *Nano Energy* **2018,** *44*, 327-335.

12. Bommier, C.; Surta, T. W.; Dolgos, M.; Ji, X., New Mechanistic Insights on Na-Ion Storage in Nongraphitizable Carbon. *Nano Letters* **2015,** *15* (9), 5888-5892.

13. Gomez-Martin, A.; Martinez-Fernandez, J.; Ruttert, M.; Winter, M.; Placke, T.; Ramirez-Rico, J., Correlation of Structure and Performance of Hard Carbons as Anodes for Sodium Ion Batteries. *Chemistry of Materials* **2019,** *31* (18), 7288-7299.

14. Qiu, S.; Xiao, L.; Sushko, M. L.; Han, K. S.; Shao, Y.; Yan, M.; Liang, X.; Mai, L.; Feng, J.; Cao, Y.; Ai, X.; Yang, H.; Liu, J., Manipulating Adsorption-Insertion Mechanisms in Nanostructured Carbon Materials for High-Efficiency Sodium Ion Storage. *Advanced Energy Materials* **2017,** *7* (17), 1700403.

15. Hasegawa, G.; Kanamori, N.; Ozaki, J.-I.; Nakanishi, K.; Abe, T., Hard carbon anods for Na-ion batteries: toward practical use. *ChemElectroChem* **2015,** *2*, 1917-1920.

16. Zhang, B.; Ghimbeu, C. M.; Laberty, C.; Vix-Guterl, C.; Tarascon, J.-M., Correlation Between Microstructure and Na Storage Behavior in Hard Carbon. *Advanced Energy Materials* **2016,** *6* (1), 1501588.

17. Hou, H.; Qiu, X.; Wei, W.; Zhang, Y.; Ji, X., Carbon Anode Materials for Advanced Sodium-Ion Batteries. *Advanced Energy Materials* **2017,** *7* (24), 1602898.

18. Saurel, D.; Orayech, B.; Xiao, B.; Carriazo, D.; Li, X.; Rojo, T., From Charge Storage Mechanism to Performance: A Roadmap toward High Specific Energy Sodium-Ion Batteries through Carbon Anode Optimization. *Advanced Energy Materials* **2018,** *8* (17), 1703268.

19. Luo, W.; Schardt, J.; Bommier, C.; Wang, B.; Razink, J.; Simonsen, J.; Ji, X., Carbon nanofibers derived from cellulose nanofibers as a long-life anode material for rechargeable sodium-ion batteries. *Journal of Materials Chemistry A* **2013,** *1* (36), 10662-10666.

20. Simone, V.; Boulineau, A.; de Geyer, A.; Rouchon, D.; Simonin, L.; Martinet, S., Hard carbon derived from cellulose as anode for sodium ion batteries: dependence of electrochemical properties on structure. *J Energy Chem* **2016,** *25*, 761-768.

21. Yamamoto, H.; Muratsukabi, S.; Kubota, K.; Fukunishi, M.; Watanabe, H.; Kim, J.; Komaba, S., Synthesizing higher-capacity hard-carbons from cellulose for Na- and K-ion batteries. *J Mater Chem A* **2018,** *6*, 16844-16848.

22. Zhang, T.; Yang, L.; Yan, X.; Ding, X., Recent Advances of Cellulose-Based Materials and Their Promising Application in Sodium-Ion Batteries and Capacitors. *Small* **2018**, 1802444.

23. Conder, J.; Villevieille, C., How reliable is the Na metal as a counter electrode in Na-ion half cells? *Chemical Communications* **2019,** *55* (9), 1275-1278.

24. Rupp, R.; Vlad, A., On the Reliability of Sodium Metal Anodes: The Influence of Neglected Parameters. *Journal of The Electrochemical Society* **2019,** *166* (14), A3122-A3131.

25. Pfeifer, K.; Arnold, S.; Becherer, J.; Das, C.; Maibach, J.; Ehrenberg, H.; Dsoke, S., Can Metallic Sodium Electrodes Affect the Electrochemistry of Sodium-Ion Batteries? Reactivity Issues and Perspectives. *ChemSusChem* **2019,** *12* (14), 3312-3319.

26. Hwang, J.; Takeuchi, K.; Matsumoto, K.; Hagiwara, R., NASICON vs. Na metal: a new counter electrode to evaluate electrodes for Na secondary batteries. *Journal of Materials Chemistry A* **2019,** *7* (47), 27057-27065.

27. Bommier, C.; Ji, X., Electrolytes, SEI Formation, and Binders: A Review of Nonelectrode Factors for Sodium-Ion Battery Anodes. *Small* **2018,** *14* (16), 1703576.

28. Bresser, D.; Buchholz, D.; Moretti, A.; Varzi, A.; Passerini, S., Alternative binders for sustainable electrochemical energy storage - the transition to aqueous electrode processing and bio-derived polymers. *Energy & Environmental Science* **2018,** *11* (11), 3096-3127.

29. Zhao, J.; Yang, X.; Yao, Y.; Gao, Y.; Sui, Y. M.; Zou, B.; Ehrenberg, H.; Chen, G.; Du, F., Moving to Aqueous Binder: A Valid Approach to Achieving High-Rate Capability and Long-Term Durability for Sodium-Ion Battery. *Advanced Science* **2018,** *5* (4), 1700768.

30. Dahbi, M.; Nakano, T.; Yabuuchi, N.; Ishikawa, T.; Kubota, K.; Fukunishi, M.; Shibahara, S.; Son, J.-Y.; Cui, Y.-T.; Oji, H.; Komaba, S., Sodium carboxymethyl cellulose as a potential binder for hard-carbon negative electrodes in sodium-ion batteries. *Electrochemistry Communications* **2014,** *44*, 66-69.

31. Fan, Q. J.; Zhang, W. X.; Duan, J.; Hong, K. L.; Xue, L. H.; Huang, Y. H., Effects of binders on electrochemical performance of nitrogen-doped carbon nanotube anode in sodium-ion battery. *Electrochimica Acta* **2015,** *174*, 970-977.

32. Darjazi, H.; Staffolani, A.; Sbrascini, L.; Bottoni, L.; Tossici, R.; Nobili, F., Sustainable Anodes for Lithium- and Sodium-Ion Batteries Based on Coffee Ground-Derived Hard Carbon and Green Binders. *Energies* **2020,** *13* (23).

33. Komaba, S.; Ishikawa, T.; Yabuuchi, N.; Murata, W.; Ito, A.; Ohsawa, Y., Fluorinated Ethylene Carbonate as Electrolyte Additive for Rechargeable Na Batteries. *Acs Applied Materials & Interfaces* **2011,** *3* (11), 4165-4168.

34. Scherrer, P., Bestimmung der Grösse und der inneren Struktur von Kolloidteilchen mittels Röntgenstrahlen. *Gött. Nachr* **1918,** *2*, 98-100.

35. Moussa, G.; Matei Ghimbeu, C.; Taberna, P.-L.; Simon, P.; Vix-Guterl, C., Relationship between the carbon nano-onions (CNOs) surface chemistry/defects and their capacitance in aqueous and organic electrolytes. *Carbon* **2016,** *105*, 268-277.

36. Beda, A.; Rabuel, F.; Morcrette, M.; Knopf, S.; Taberna, P. L.; Simon, P.; Matei Ghimbeu, C., Hard Carbon Key Properties Allow for the Achievement of High Coulombic Efficiency and High Volumetric Capacity in Na-Ion Batteries. *J Mater Chem A* **2021,** *9*, 1743-1758

37. del Mar Saavedra Rios, C.; Simonin, L.; de Geyer, A.; Matei Ghimbeu, C.; Dupont, C., Unraveling the Properties of Biomass-Derived Hard Carbons upon Thermal Treatment for a Practical Application in Na-Ion Batteries *Energies* **2020,** *13(14)*, 3513.

38. Izanzar, I.; Dahbi, M.; Kiso, M.; Doubaji, S.; Komaba, S.; Saadoune, I., Hard carbons issued from date palm as efficient anode materials for sodium-ion batteries. *Carbon* **2018,** *137*, 165-173.

39. Cao, Y.; Xiao, L.; Sushko, M. L.; Wang, W.; Schwenzer, B.; Xiao, J.; Nie, Z.; Saraf, L. V.; Yang, Z.; Liu, J., Sodium Ion Insertion in Hollow Carbon Nanowires for Battery Applications. *Nano Letters* **2012,** *12* (7), 3783-3787.

40. Rios, C. D. S.; Simonin, L.; de Geyer, A.; Ghimbeu, C. M.; Dupont, C., Unraveling the Properties of Biomass-Derived Hard Carbons upon Thermal Treatment for a Practical Application in Na-Ion Batteries. *Energies* **2020,** *13* (14), 3513.

41. Conder, J. M.; Vaulot, C.; Marino, C.; Villevieille, C.; Ghimbeu, C. M., Chitin and chitosan – structurally-related precursors of dissimilar hard carbons for Na-ion battery. *ACS Applied Energy Materials* **2019,** *2*, 4841–4852.

42. Matei Ghimbeu, C.; Zhang, B.; Martinez de Yuso, A.; Rety, B.; Tarascon, J.-M., Valorizing low cost and renewable lignin as hard carbon for Na-ion batteries: Impact of lignin grade. *Carbon* **2019,** *153*, 634-647.

43. Komaba, S.; Murata, W.; Ishikawa, T.; Yabuuchi, N.; Ozeki, T.; Nakayama, T.; Ogata, A.; Gotoh, K.; Fujiwara, K., Electrochemical Na Insertion and Solid Electrolyte Interphase for Hard-Carbon Electrodes and Application to Na-Ion Batteries. *Advanced Functional Materials* **2011,** *21* (20), 3859-3867.

44. Morikawa, Y.; Nishimura, S.; Hashimoto, R.; Ohnuma, M.; Yamada, A., Mechanism of Sodium Storage in Hard Carbon: An X-Ray Scattering Analysis. *Advanced Energy Materials* **2020,** *10* (3), 1903176.

45. Stevens, D.; Dahn, J. R., The mechanisms of lithium and sodium insertion in carbon materials. *J Electrochem. Soc* **2001,** *148*, A803-A811.

46. Stratford, J. M.; Allan, P. K.; Pecher, O.; Chater, P. A.; Grey, C. P., Mechanistic insights into sodium storage in hard carbon anodes using local structure probes. *Chemical Communications* **2016,** *52* (84), 12430-12433.

47. Eshetu, G. G.; Grugeon, S.; Kim, H.; Jeong, S.; Wu, L. M.; Gachot, G.; Laruelle, S.; Armand, M.; Passerini, S., Comprehensive Insights into the Reactivity of Electrolytes Based on Sodium Ions. *Chemsuschem* **2016,** *9* (5), 462-471.

48. Fondard, J.; Irisarri, E.; Courreges, C.; Palacin, M. R.; Ponrouch, A.; Dedryvere, R., SEI Composition on Hard Carbon in Na-Ion Batteries After Long Cycling: Influence of Salts (NaPF6, NaTFSI) and Additives (FEC, DMCF). *Journal of the Electrochemical Society* **2020,** *167* (7), 070526.

49. Frost, R.; Hales, M.; Martens, W., Thermogravimetric analysis of selected group (II) carbonate minerals-implication for the geosequestaration of greenhouse gases. *J Therm Anal Calor* **2009,** *95*, 999-1005.

50. Hourlier, D., Thermal decomposition of calcium oxalate: beyond appearances. *Journal of Thermal Analysis and Calorimetry* **2019,** *136*, 2221-2229.

51. Huang, S.; Li, Z.; Wang, B.; Zhang, J.; Peng, Z.; Qi, R.; Wang, J.; Zhao, Y., N-Doping and Defective Nanographitic Domain Coupled Hard Carbon Nanoshells for High Performance Lithium/Sodium Storage. *Advanced Functional Materials* **2018,** *28* (10), 1706294.

52. Li, Z.; Chen, Y.; Jian, Z.; Jiang, H.; Razink, J. J.; Stickle, W. F.; Neuefeind, J. C.; Ji, X., Defective Hard Carbon Anode for Na-Ion Batteries. *Chemistry of Materials* **2018,** *30* (14), 4536-4542.

53. Yu, K. H.; Wang, X. R.; Yang, H. Y.; Bai, Y.; Wu, C., Insight to defects regulation on sugarcane waste-derived hard carbon anode for sodium-ion batteries. *Journal of Energy Chemistry* **2021,** *55*, 499-508.

54. Alvin, S.; Yoon, D.; Chandra, C.; Cahyadi, H. S.; Park, J. H.; Chang, W.; Chung, K. Y.; Kim, J., Revealing sodium ion storage mechanism in hard carbon. *Carbon* **2019,** *145*, 67-81.

55. Chen, D.; Zhang, W.; Luo, K.; Song, Y.; Zhong, Y.; Liu, Y.; Wang, G.; Zhong, B.; Wu, Z.; Guo, X., Hard carbon for sodium storage: mechanism and optimization strategies toward commercialization. *Energy & Environmental Science* **2021,** *14* (4), 2244-2262.

56. Chen, X.; Fang, Y.; Tian, J.; Lu, H.; Ai, X.; Yang, H.; Cao, Y., Electrochemical Insight into the Sodium-Ion Storage Mechanism on a Hard Carbon Anode. *Acs Applied Materials & Interfaces* **2021,** *13* (16), 18914-18922.

57. Memarzadeh Lotfabad, E.; Kalisvaart, P.; Kohandehghan, A.; Karpuzov, D.; Mitlin, D., Origin of non-SEI related coulombic efficiency loss in carbons tested against Na and Li. *J. Mater. Chem. A* **2014,** *2* (46), 19685-19695.